

# CARBON NANOTUBES AS ELECTRON SOURCES

*M. Mann\*, K.B.K. Teo, W.I. Milne*

**Cambridge University Engineering Department, Cambridge, UK**

**Contact email: [mm354@cam.ac.uk](mailto:mm354@cam.ac.uk)**

Electron sources are employed in a wide range of technologies which include displays [1], telecommunication devices [2], electron-beam imaging equipment [3], microwave amplifiers [4] and even electric-propulsion systems for spacecraft [5]. The most widely employed electron source is still the thermionic cathode used in television cathode-ray tubes and high-power microwave amplifiers, though its popularity is on the decline with the advent of flat-panel displays. Thermionic emission occurs when a charged metal or a charged metal oxide surface is heated. The thermal vibrational energy gained by the electrons overcomes the electrostatic forces holding them to the surface. The electrons are released into vacuum from the surface and the resultant beam being controlled by a sequence of fields. The temperature of operation is typically 2000 K; an undesirable attribute as this results in an inefficient consumption of power. The vacuum tube required is also quite large – in the case of displays, as long as the display is wide – which has also contributed to its decline in popularity. Demand has pushed the requirements of the electron source to smaller and smaller scales to increase efficiency and to open up opportunities for alternative electron source applications. As well as flat-panel displays, new applications include parallel electron-beam microscopy and nanolithography, compact microwave amplifiers and portable X-ray tubes have motivated worldwide research into alternative smaller, more efficient electron source technologies.

Field emission, also known as Fowler-Nordheim tunnelling, is a form of quantum mechanical tunnelling in which electrons pass through a barrier in the presence of a high electric field. Field emission offers a route to smaller, more efficient electron source technologies. The phenomenon is highly dependent on both the properties of the material and the shape of the cathode; high aspect ratios produce higher field emission currents. In contrast to the commonly used thermionic emission based on a hot filament, field emission occurs at or close to room temperature from an unheated ‘cold’ cathode under the influence of an electric field.

Consequently, field emitters are more power-efficient than the heated thermionic emitter. Also, field emission sources offer several attractive characteristics such as instantaneous response to field variation, resistance to temperature fluctuation and radiation, a high degree of coherence in electron optics, a good on/off ratio, ballistic transport and a nonlinear current-voltage relationship in which a small change in voltage results in a large change in emission current. However, to extract a current significant enough to be used for the aforementioned applications, field emission requires a very large local field of a few V/nm. A typical method employed to attain this high field is to use a very sharp needle, such as tungsten, with the apex chemically etched to a few hundred nanometres. Even so, with this geometry, a few thousand volts still needs to be applied macroscopically in order to draw a useable current (e.g. the extraction voltage of a field emission electron microscope is 1-5 kV). Recently developed micro and nano-fabrication techniques have allowed for the extraction electrode to be positioned much closer to the tip and for the apex of the needle to be etched to increasingly smaller diameters. Both these factors lead to a higher field concentration at the tip, reducing the extraction voltage by as much as an order of magnitude. This has spurred on the development of ‘sharp’ protruding microstructures, the most famous of which is the Spindt tip cathode which was invented in the late 1960’s [6]. The Spindt tip cathode has been successfully used in prototypes for flat panel displays and microwave amplifiers as shown in Fig. *Error! No text of specified style in document.****1***.

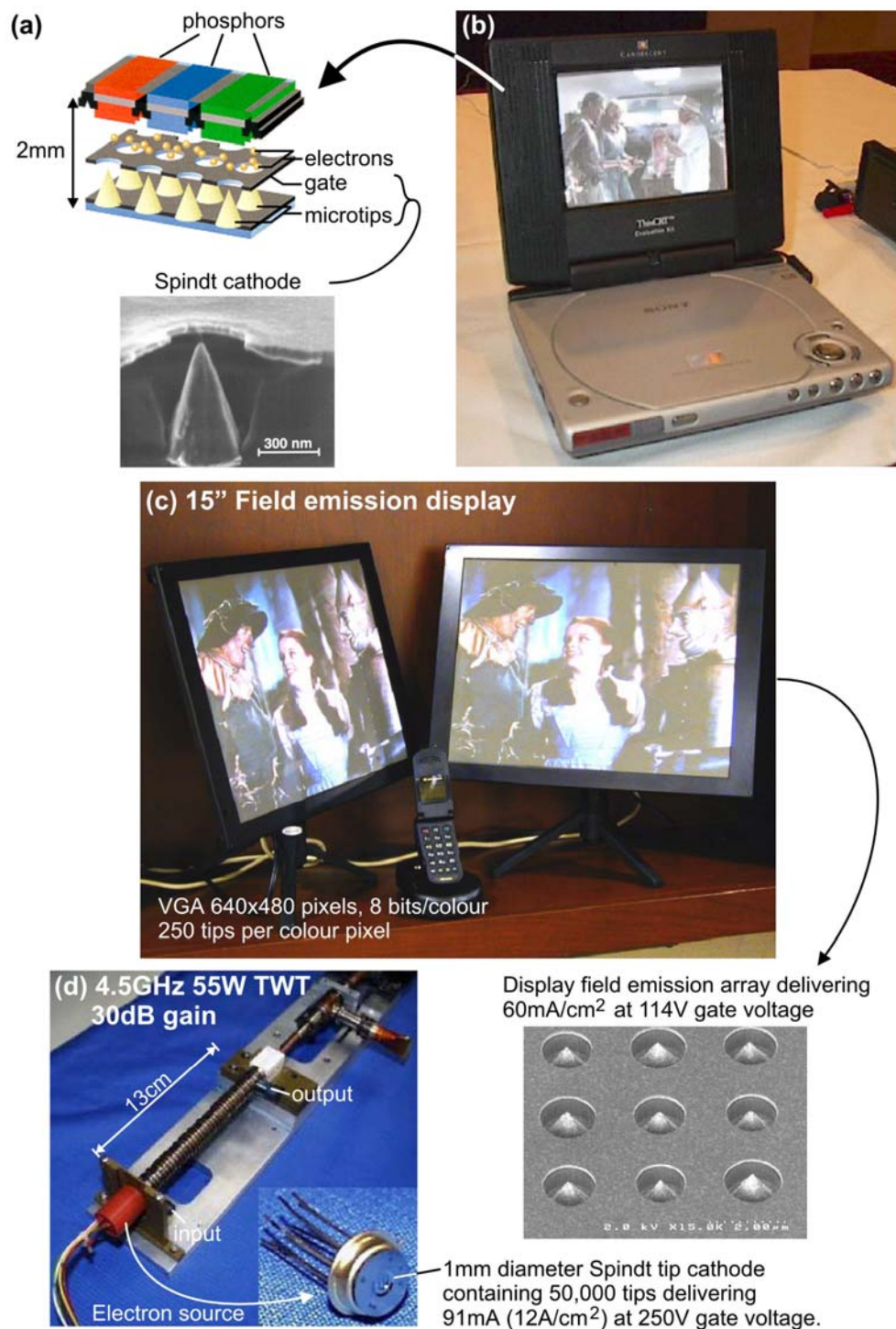


**Fig. Error! No text of specified style in document.1.** (a) Cross-section of a field emission display [7] showing a Candescent Spindt tip cathode [8], (b) Sony portable DVD player using a Candescent field emission display [9] (c) Motorola 15" field emission display [9], and (d) Northrop-Grumman microwave amplifier using SRI Spindt tip cathode [9,10]. Figures reprinted with permission from AIP, IEEE and K.L. Jensen. © 2000 American Institute of Physics. © 1991 IEEE.

## 1.1 THE FIELD EMISSION PROCESS

Field emission is the quantum-mechanical tunnelling of electrons from a surface into vacuum in response to a very high electric field. In a material, electrons at the Fermi level must in general overcome the potential barrier imposed by the work function ( $\phi$ ) before they can escape into vacuum. In the presence of an external electric field, the external potential barrier  $V(x)$  is modified as shown in Figure 1.1.1. For typical metals ( $\phi = 4.5$  eV), field emission occurs when the barrier width is reduced to a few nanometres under an applied electric field,  $E_{local}$ , of a few V/nm. Due to the quantum-mechanical uncertainty in the electron position, electrons are able to tunnel across this narrow barrier. As the field increases, the barrier width decreases resulting in more electrons tunnelling across the barrier. Typically, detectable tunnelling current occurs where  $E_{local} > 3$  V/nm.

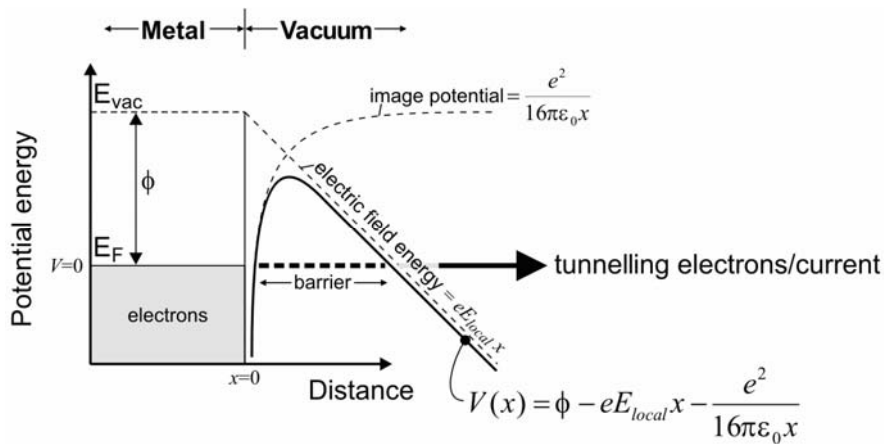


**Fig. 1.1.1.** A diagram representing the band structure showing the tunnelling of free electrons at the Fermi level (for a metal-like material) through an electric field-narrowed potential barrier.

For any material, the tunnelling current density is given by integrating the product of the electron transmission probability through the barrier,  $T(E)$ , and the incident supply of electrons,  $N(E)$ , over the range of potential energies. Physically,  $T(E)$  depends on the barrier width, which in turn depends on the field applied and the work function of the material.  $N(E)$  depends on the band structure of the material and the distribution of electrons at a particular temperature. By assuming a metallic free-electron band structure at 0 K, the emission current follows the Fowler-Nordheim law [11]:

$$J = \frac{A_{FN}}{\phi t^2(y)} E_{local}^2 \exp\left(\frac{-B_{FN} \phi^{1.5}}{E_{local}} \nu(y)\right) \quad (1.1)$$

where  $J$  = current density or current per unit area in  $A/cm^2$

$$A_{FN} = \frac{e^3}{8\pi h} = 1.54 \times 10^{-6} \text{ A eV V}^{-2}$$

$$B_{FN} = \left(\frac{8\pi}{3}\right) \left(\frac{\sqrt{2m}}{eh}\right) = 6.83 \times 10^7 (\text{eV})^{-1.5} \text{ V (cm)}^{-1}$$

evaluated using

$e$  = electronic charge ( $1.602 \times 10^{-19}$  C),

$h$  = Planck's constant ( $6.626 \times 10^{-34}$  J s),  $m$  = electron mass ( $9.11 \times 10^{-31}$  kg)

$t(y)$ ,  $\nu(y)$  = Nordheim elliptic functions where  $y = \sqrt{\frac{e^3 E_{local}}{4\pi\epsilon_0 \phi^2}}$

$\epsilon_0$  = permittivity of free space ( $8.854 \times 10^{-12}$  F/m)

$\phi$  = work function of the emitter in eV, and,

$E_{local}$  = applied local electric field in V/cm.

Reference [12] provides a good account of the development of the original Fowler-Nordheim equation through modern times. A useful simplification of the Fowler-Nordheim law is arrived at by the approximations  $t(y) = 1.1$  and  $\nu(y) = 0.95 - y^2$  which was proposed by Brodie and Spindt [13], yielding the following equation:

$$J = \frac{1.5 \times 10^{-6}}{\phi} E_{local}^2 \exp\left(\frac{10.4}{\sqrt{\phi}}\right) \exp\left(\frac{-6.44 \times 10^7 \phi^{1.5}}{E_{local}}\right) \quad (1.2)$$

For a fixed material, the work function  $\phi$  is usually known and hence the emission current density ( $J$  = current/area) can be expressed as a function  $E_{local}$ . It is also immediately apparent that in order to extract larger currents, either  $E_{local}$  must be increased or  $\phi$  decreased. To increase  $E_{local}$ , one uses large geometrical field enhancement structures (e.g. sharp tips) such that  $E_{local} = \beta \times E_{applied}$ , where  $\beta$  is the field enhancement factor and

$E_{applied}$  is the electric field applied macroscopically. To decrease  $\phi$ , the cathode can be coated with a lower work function material such as Cs ( $\phi = 1.9$  eV) or Ba ( $\phi = 2.3$  eV), compared with W ( $\phi \cong 4.5$  eV) and Mo ( $\phi = 4.5$  eV). An issue to bear in mind is that low work function materials usually have lower melting points (Cs = 28 °C, Ba = 725 °C) than high work function materials (W = 3410 °C, Mo = 2620 °C) which are consequently more stable at higher temperatures. Some low work function oxides (eg. CsO, BaO, ZrO) are also used as work function lowering coatings.

Brodie and Spindt [13] proposed a final simplification to equation (1.2) in order to conveniently describe field emission from gated arrays of microcathodes. This is done by substituting  $J = I/Area$  (where  $I$ =total current in amps,  $Area$ =apparent emission area in  $cm^2$ ) and  $E_{local} = \gamma V$  (where  $V$  is the applied gate voltage in volts,  $\gamma$  is the cathode geometry dependent field-forming factor in V/cm) to arrive very simply at:

$$I = aV^2 \exp(-b/V) \quad (1.3)$$

$$\text{where } a = Area \times \frac{1.5 \times 10^{-6}}{\phi} \gamma^2 \exp\left(\frac{10.4}{\sqrt{\phi}}\right) \text{ in Amps } V^{-2}, \text{ and,}$$

$$b = \frac{6.44 \times 10^7}{\gamma} \phi^{1.5} \text{ in Np } V.$$

Therefore, by measuring the I-V characteristics of microcathodes and fitting them to equation 1.3, it is now possible to compare their performance by using their ‘ $a$ ’ and ‘ $b$ ’ parameters.

## 1.2 CARBON MATERIALS FOR FIELD EMISSION

High melting point metals such as molybdenum or tungsten are the materials most commonly used for field emission tips. In recent years, silicon has also been used for field emitter arrays because of the widespread availability of silicon micro-fabrication techniques.

One of the earliest reports of carbon being used as an emission source was by Baker [14] in 1972 who noticed that graphite fibres showed better stability than several metals in a number of environments. In 1991, Wang [15] and Geis [16] reported field-emission at a low threshold ( $<3 \text{ V}/\mu\text{m}$ ) from diamond-based cathodes. In the same year, Djuba [17] also showed that arrays of diamond-like carbon (DLC) cones emitted at lower operating voltages than arrays of molybdenum or hafnium tips. These works initiated further and more extensive research into field-emission from carbon materials.

More recently, favourable electron emission properties have been reported from diamond deposited by chemical vapour deposition (CVD) [18], amorphous diamond-like carbon [19,20], graphite grown by CVD [21] containing carbon nanotubes (CNTs) [22,23], nanocrystalline nanocomposite (do you mean nanocrystalline?)graphitic carbon [24], nanostructured carbon [25], carbon [26], and polymers [27]. These materials are technologically important because relatively good electron emission properties can be obtained when these materials are directly deposited onto a flat electrode/surface, thus removing the need to fabricate the tip.

In the early 1990's, one could class these carbon materials into 2 distinct types based on their proposed emission mechanism –

- (1) the structured graphitic ( $\text{sp}^2$ ) classes of carbons where emission is from field enhancement of the conductive structures, and
- (2) the diamond-type ( $\text{sp}^3$ ) classes of carbons where emission is enhanced by negative electron affinity (NEA) [28,29] or band bending effects [20,30].

The original concept behind using a wide band gap material like diamond or DLC was that its electron affinity (i.e. difference in vacuum level to conduction band level) was negative or low. Thus, to make use of this, electrons would have to be injected into the conduction band of the wide band gap material and these electrons would then see a reduced potential barrier (due to low/negative electron affinity) and easily emit into vacuum. It is now generally accepted that this does not occur. Such NEA/band-bending effects would apply over a homogeneous

diamond/DLC coating to produce uniform emission across the whole surface, and yet the observed field emission always occurred as a handful of randomly distributed emission sites (see [10,31] for example). The inhomogeneous nature of field emission sites indicated that there was something peculiar about the emission sites in relation to the rest of the carbon coating.

In the case of CVD diamond coatings, simultaneous photoemission and field emission spectroscopy studies showed that the field emitted electrons originated from ~5-6 eV below the vacuum level and had local fields of the order of 2-3 V/nm, even whilst the diamond film exhibited NEA [32]. This shows that conventional field-enhancement type emission was occurring from specific sites on the CVD diamond surface. Studies by scanning probe microscopy further showed that the emission originated from the conductive, graphitic grain boundaries of CVD diamond [33]. Furthermore, it was found that if the diamond film contained more defects/grain boundaries (e.g. in fine grain/nanocrystalline diamond), the material exhibited better field emission properties [18,31], confirming the fact that the good field emission properties of CVD diamond was a result of highly conductive, sharp edged (for high field enhancement) grain boundaries.

A similar story was also emerging for DLC – the following discussion outlines a particular type of DLC known as tetrahedral amorphous carbon (ta-C) which was much investigated in the literature for electron emission. From the authors' own experience, not a single emission site was observed from a thin, flat film of high band gap (3.6 eV) essentially macroparticle-free (<0.01% coverage) ta-C when fields of 50-100 V/ $\mu\text{m}$  were applied. Other researchers [34,35] found that with similar high quality ta-C thin films, field emission only occurred after a vacuum arc discharge event at applied fields of 80-180 V/ $\mu\text{m}$  (sometimes called 'activation'). Post-experimental scanning electron microscopy (SEM) of these ta-C coatings revealed craters or hill-like formations which corresponded to the emission sites [34,35] - it is conceivable that field enhancement from these protrusions caused the detected field emission. There were still other works [24,36] which reported field emission from as-deposited 'flat' ta-C films, but SEM observation of these films showed that they were littered with micron-sized graphitic particles (see ref. [37]).

Simultaneous photoemission and field emission spectroscopy studies on ta-C showed that the field emitted electrons originated from 5eV below the vacuum level at local fields of 6.5V/nm and from structures with  $\beta = 150-300$  [38]. It is thus believed that the edges/facets of graphitic particles could be responsible for high local field enhancement which gave rise to conventional field emission. Tsai et al. [39] used an in-situ microscope to examine ta-C films similar to ref. [24] during field emission measurements and have shown conclusively that the electron emission originated from graphitic micro-particles. In fact, as it was now apparent that field enhancement from local structures was responsible for the electron emission, there was no need to produce clean, high band gap ta-C films as 'flat' field emission sources. The new trend was to produce composite carbon films rich in graphitic nanostructures. Such films could easily be deposited with an unfiltered cathodic arc in a high pressure environment (e.g. with N<sub>2</sub>/He) [23,24,25]. These films contained a plethora of graphitic nano-particles, onions, clusters, cauliflowers and nanotubes, and exhibited relatively 'good' field emission properties with low applied macroscopic turn-on fields of 1-5 V/ $\mu\text{m}$ .

It is therefore safe to conclude that carbon films structurally rich in the micro/nanoscale perform very well as field emission sources. The presence of 'sharp' conductive graphitic structures, be they nanotubes, grain boundaries or graphite particles, provide the necessary electron supply and geometrical enhancement for conventional Fowler-Nordheim field emission to occur. It should be noted that these field enhancement structures occur 'naturally' in the deposited carbon films, in contrast to fabricated metal tips.

Also, there are several physical properties of carbon-based emitters which are more favourable than metal emitters. Diamond and graphite-based emitters have high melting points (>3000K) in vacuum, and are inert/stable in most common acids and alkalis (which would ease processing). The carbon films based around a diamond-like matrix are also mechanically robust. Even free-standing nanotubes/nanofibers on a substrate have been reported to survive the rigours of 'semiconductor' processing such as being coated with insulator or submitted to reactive ion etching [40,41].

### 1.3 MOTIVATION FOR CARBON NANOTUBE EMITTERS

Carbon nanotubes are a unique form of carbon filament/fibre in which the graphene walls roll up to form tubes [42]. There are several properties of carbon nanotubes which make them extraordinary materials for field emission.

Firstly, the graphene walls in them are parallel to the filament axis resulting in the nanotubes (whether metallic single-walled or multi-walled) exhibiting high electrical conductivity at room temperature.

Secondly, nanotubes are high in aspect ratio and whisker-like in shape. Utsumi [43] evaluated commonly used field emission tip shapes as shown in Fig. 1.3.1, and concluded that the best field emission tip should be whisker-like, followed by the sharpened pyramid, hemi-spheroidal, and pyramidal shapes. Indeed, nanotubes are whisker-like. It has been reported that even curly ‘spaghetti-like’ nanotubes stand up vertically like whiskers during emission under the application of an electric field [44].

Thirdly, nanotubes can be very stable emitters, even at high temperatures. Purcell et al. [45] demonstrated that a multi-walled carbon nanotube emitter could be heated up by its field-emitted current up to 2000K and remain stable. They claimed that this was the first reported observation of field emission induced stable heating. This characteristic is distinctively different from metal emitters. In metals, the resistance,  $R$ , increases with temperature, which means that more heat,  $Q$ , is produced as higher currents,  $I$ , are drawn ( $Q = I^2R$ ). The combination of high temperature and electric field causes the well known mechanism of field-sharpening of tips by surface diffusion, which in turn increases the local field, current and temperature. This positive feedback mechanism causes an unstable thermal runaway which inevitably leads to emitter destruction for metal-based emitters. In contrast, the resistance of a nanotube decreases with temperature which limits  $I^2R$  heat generation. Consequently, its temperature varies sub-linearly with current [46]. Added to this, surface diffusion is less likely in the strong C-C covalent bonds of the carbon

nanotube. These unique characteristics of carbon nanotubes make them remarkable field emitters.

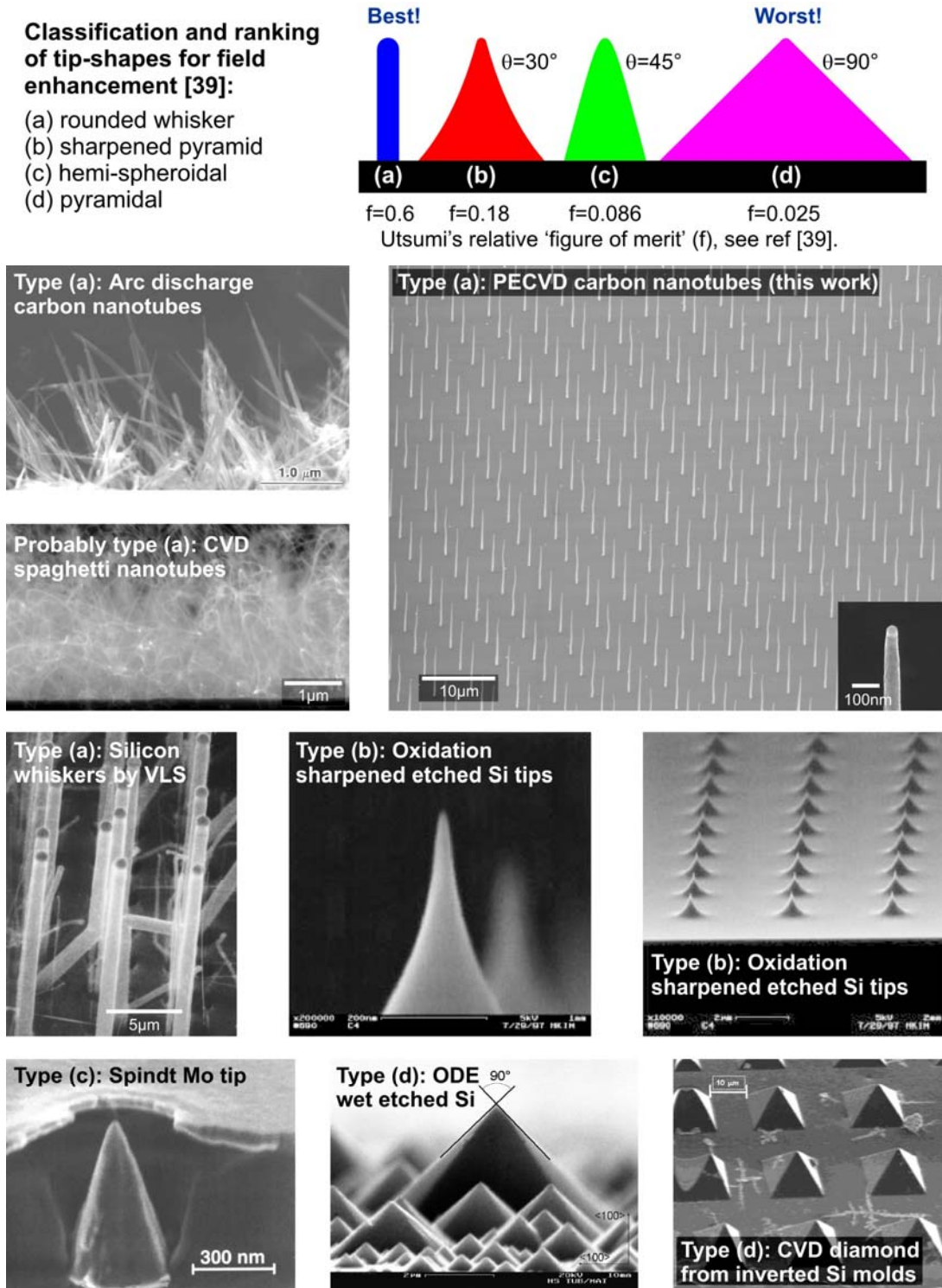


**Fig. 1.3.1.** Classification and ranking of tip-shapes proposed by Utsumi [43]. From best to worst - (a) rounded whisker which is ideal, (b) sharpened pyramid, (c) hemi-spheroidal, and (d) pyramidal [45]. Figures

reprinted with permission from AIP and IEEE. © 1991 IEEE. © 2000, 1997, 1993 American Institute of Physics.

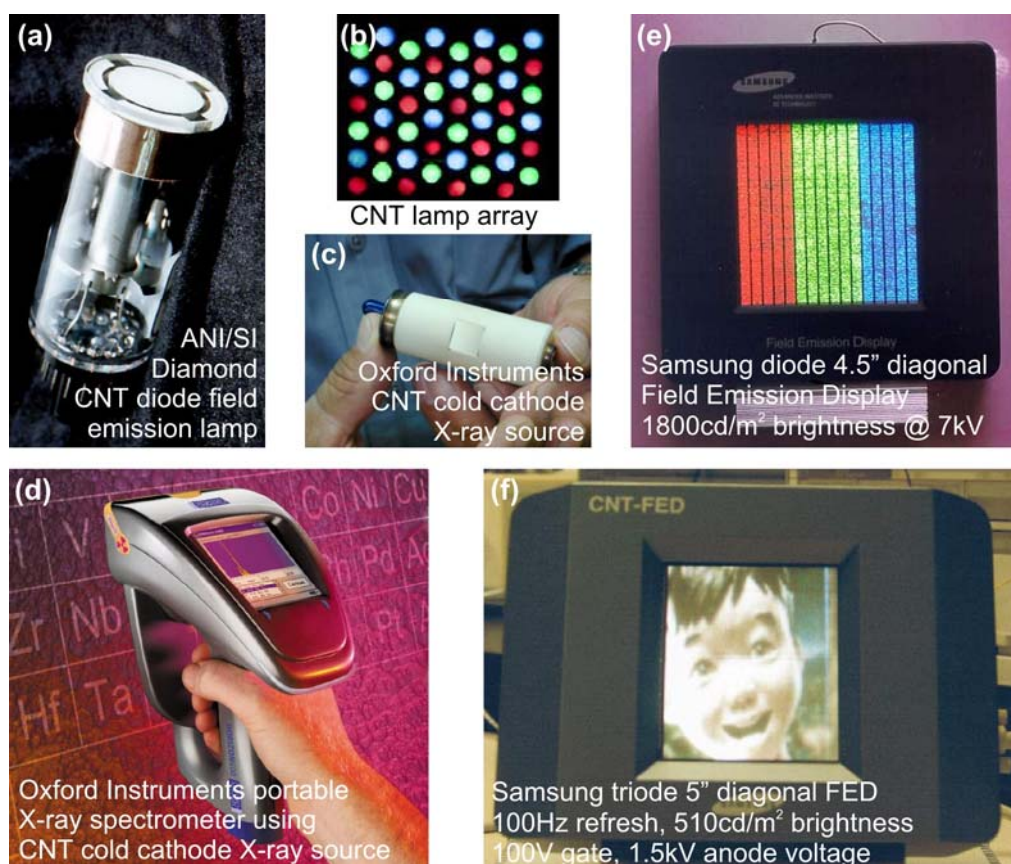


**Fig. 1.3.2.** Applications, such as lamps, X-ray source and field emission displays, using carbon nanotubes (CNT) as the field emission electron source [47]. Figures reprinted with permission from AIP. © 1999 American Institute of Physics.

In most applications today (Fig. 1.3.2), nanotubes are first mass produced by arc-discharge as this is presently the most cost-effective production technique [48]. The arc discharge nanotubes are purified and mixed with an epoxy/binder, and then screen printed or applied at emitter locations, such as that used in [47]. Alternatively, electrophoresis can be used to adhere the arc discharge nanotubes in solution to specific electrodes [49]. Practically speaking, these strategies are useful only for ‘macroscopic’ field emission sources, such as those used in the applications of Fig. 1.3.2, because the carbon nanotubes are ‘randomly’ distributed and unoriented as shown in the SEM of arc discharge nanotubes of Fig. 1.1a.

What research groups have been focusing on in more recent work is the controlled production of micro-field emission sources based on carbon nanotubes. Such electron sources could be used in microguns for electron microscopy and parallel electron beam lithography, but are also equally applicable to ‘macroscopic’ applications such as field emission displays, microwave amplifiers and X-ray sources. From 1999, various catalytic chemical vapour deposition (CVD) methods were developed as a means of controlling the direct deposition of carbon nanotubes, where required, onto a substrate. It is first important to grasp the fundamentals of PECVD growth, which are outlined in the next section.

#### **1.4 GROWTH OF CARBON NANOTUBES**

There are two basic techniques used for CNT synthesis, vaporization of graphite or chemical vapour deposition. There are the two vaporization methods: arc discharge [50] and laser ablation [51] and vaporization tends to be favoured for bulk CNT growth. In the arc discharge method, an electric spark between two carbon (usually graphite) rods (typically 100 A) sublimates the carbon in the negative electrode because of the high temperature of the discharge. The vaporized carbon then goes on to form CNTs. Laser ablation involves a pulsed laser that vaporizes a graphite target in a high temperature reactor. Inert gas is bled into the chamber with the CNTs forming on the cooler surfaces of the reactor. For more detail on these methods see references [50] and [51]. The CNTs produced are often coated in layers of amorphous carbon (70% amorphous carbon for arc discharge, 30% amorphous carbon for laser ablation [52]), so a purification step is required to separate the CNTs from the amorphous carbon. CNTs made in this way have been applied to field emission displays, but this synthesis method will not be discussed in detail here, as researchers making devices tend to favour CVD.

The CVD process is a two step process and these are:

- (1) preparation of catalyst nanoparticles and
- (2) growth of the nanotubes by CVD or PECVD (plasma-enhanced chemical vapour deposition), as will be described below.

### 1.4.1 GROWTH BY PLASMA-ENHANCED CHEMICAL VAPOUR DEPOSITION

The catalyst metals commonly used for nanotube growth are Fe, Ni and Co [53]. There are several routes to the production of catalyst nanoparticles, such as the wet catalyst method, etching of catalyst metal and coalescence of thin catalyst films.

The wet catalyst method and the etching method are summarised in Figures 1.4.1(a) and (b) respectively, but the most commonly used form of catalyst preparation for devices is coalescence (shown in figure 1.4.1c).

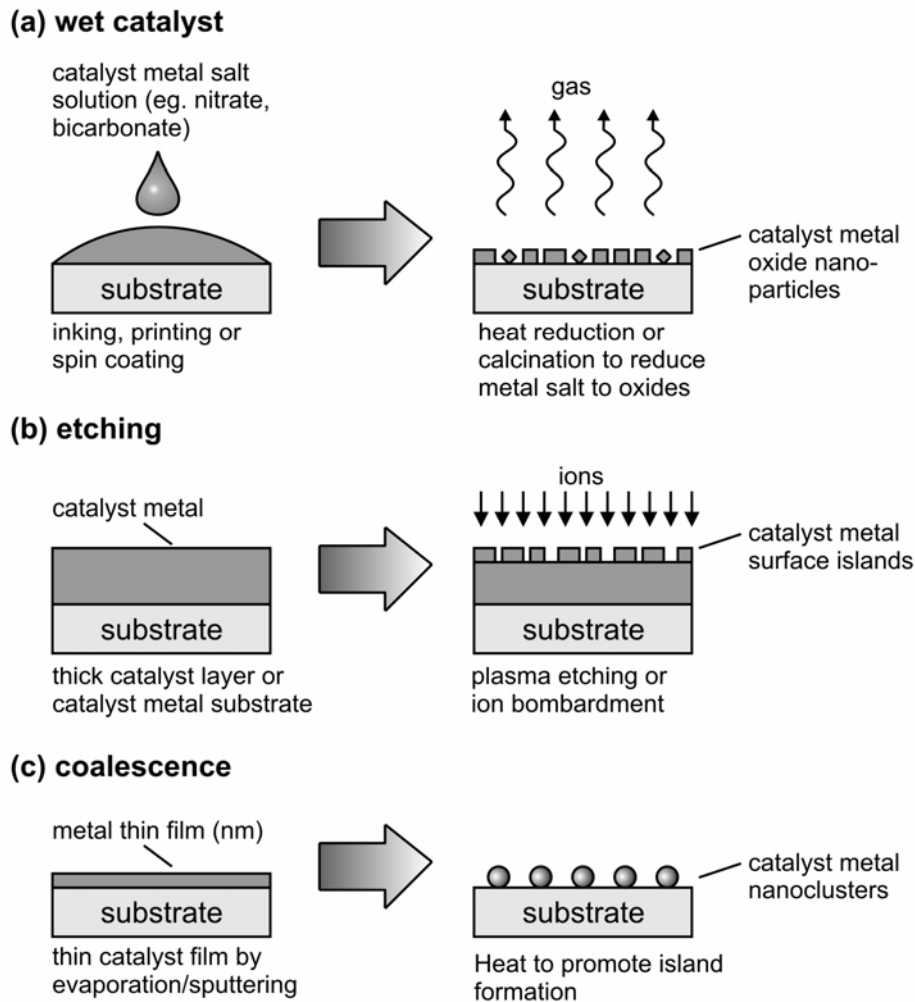


**Fig. 1.4.1.** Methods of producing nano-sized catalysts for nanotube growth.

A very thin film of Fe, Co or Ni is carefully deposited on a substrate using R.F. magnetron sputtering or evaporation. A typical film thickness would be a few nanometres with the thickness monitored during deposition by a quartz film thickness monitor. When this thin film is heated up to a high temperature (such as the growth temperature), the thin film breaks up (known as dewetting) and agglomerates to form nanoclusters due to increased surface mobility and the strong cohesive forces of the metal atoms [54,55]. These nanoclusters then catalyze the growth of the carbon nanotubes.

### 1.4.2 GROWTH BY CVD AND PECVD

After catalyst nanoclusters have formed, the second step of the process is nanotube growth by CVD or PECVD. This is typically performed using a mixture of a deposition gas (eg. carbon containing gas such as  $C_2H_2$ ,  $CH_4$ , or  $CO$ ) and an etching/reducing gas (e.g.  $H_2$  or  $NH_3$ ) at a temperature of  $550-900^\circ C$ .

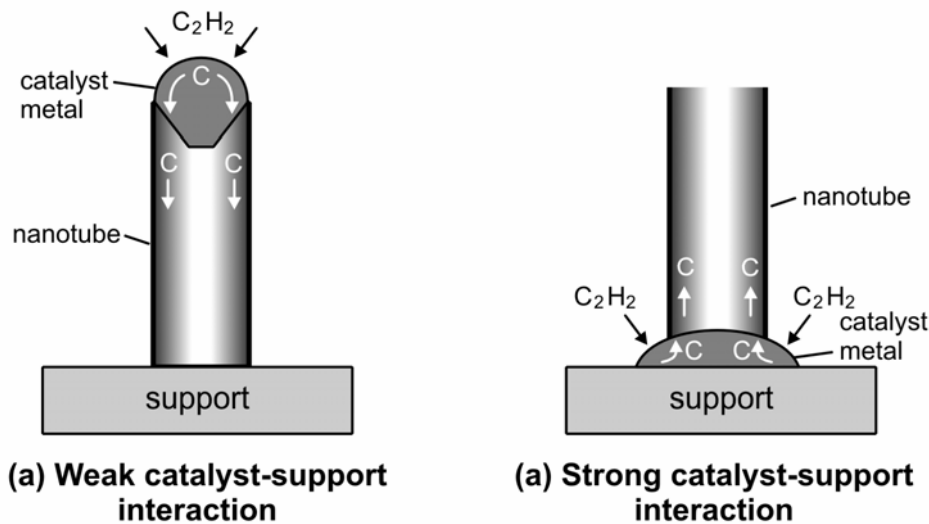


**Fig. 1.4.2.** Two types of growth, namely tip or base growth, resulting from different catalyst-support interactions [53].

The deposition gas provides the carbon feedstock for nanotube growth, and early works showed that typically temperatures in excess of  $500^\circ C$  are required for the filamentous growth of carbon via catalytic decomposition of the gas and the diffusion of carbon through the catalyst

[53]. In CVD, the energy required to break down the reactant deposition gases into graphene comes solely from the heat supplied to the catalyst particle and its immediate environs. There is no alignment of CNTs as a result of the CVD process. In PECVD, the plasma creates a sheath above the substrate in which an electric field perpendicular to the substrate is induced. This field breaks down some of the deposition gases and vertically aligns the nanotubes during growth. As depicted in Figure 1.4.2, two growth modes, tip or base growth, are possible based on whether the catalyst metal interacts strongly or weakly with the underlying support material. The interaction of the catalyst with the support can be characterized by its contact angle, analogous to ‘hydrophobic’ (weak interaction) and ‘hydrophilic’ (strong interaction) surfaces. For example, Ni on TiN or SiO<sub>2</sub> has contact angle  $>90^\circ$  (i.e. ‘hydrophobic’ or weak interaction) and thus tip-growth is favoured. On the other hand, Co or Fe on Si [55,56] favour base growth.

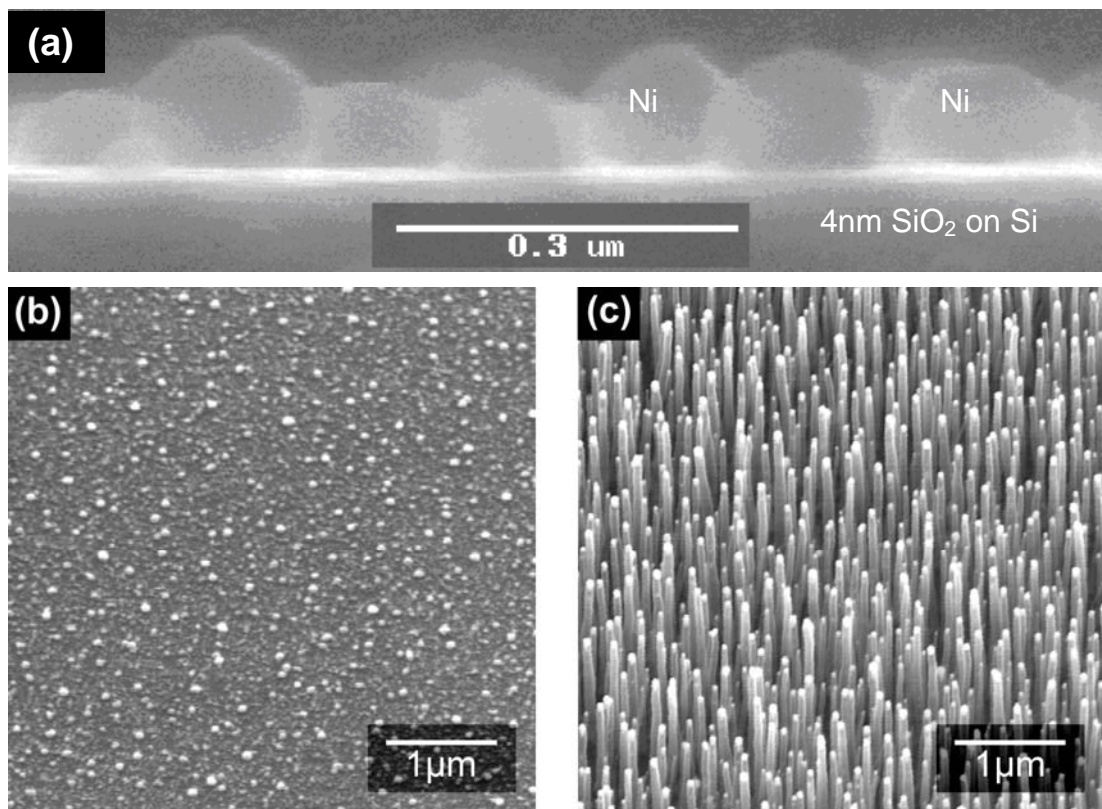


**Fig. 1.4.3.** Ni nanoclusters ((a) and (b)), when on a 4nm layer of SiO<sub>2</sub> deposited onto a Si substrate, exhibit weak interactions (c.f. ‘hydrophobic’) with their supports hence favouring tip growth (the Ni is the high contrast dot seen at the tip of the nanotube as in (c)).

For tip growth, the nanotube length increases with deposition pressure and time as the catalyst is always exposed to the incoming gas/plasma on top. In base growth, it is common for the nanotube length to saturate quickly after growth is commenced as the catalyst becomes covered by carbon layers or buried beneath a forest of nanotubes [55]. To circumvent this, special substrates such as porous Si are used to ensure that the gases can permeate through to the catalyst as demonstrated in ref. [57]. For most applications, tip growth is favoured as the dimensions of the nanotubes can be controlled more accurately (with a typical growth shown in figure 1.4.3).

## **1.5 FIELD EMISSION DEVICES THAT UTILIZE CARBON NANOTUBES**

The last part of this chapter focuses on some of the interesting applications of carbon nanotubes to devices, particularly electron beam devices, where PECVD is combined with microelectronic fabrication technology to produce uniform, well aligned and, where desired, patterned carbon nanotubes for field emission. Field emission lamps [58], gas discharge tubes [59], X-ray sources [60] and field emission displays [61] are covered in detail elsewhere and summarized by de Jonge et al. [62]. This section includes two applications covered by Milne et al. [63] and how they have progressed recently, together with their application to electron sources for microscopy.

### **1.5.1 CARBON NANOTUBES APPLIED TO GATED CATHODES FOR PARALLEL ELECTRON BEAM LITHOGRAPHY**

The “incredible shrinking microprocessor” described in Moore’s Law dictates that for advances in processing power to continue at the same rate, efficient techniques for sub-100 nm semiconductor lithography and mask production need to be found. A potential candidate is electron-beam direct write (EBDW), as sub 100 nm beam sizes are relatively straightforward to obtain. However, current EBDW utilizes only a single electron beam to write with necessitating serial writing with the

consequence of a low throughput. A possible solution to this problem and one that is a relatively straightforward concept is to use an array of parallel electron beams. For microelectron source instruments, such as those employed in parallel electron beam lithography and the miniature scanning electron microscope, a “triode” structure with an integrated extraction gate electrode is preferred. The key advantages of using carbon nanotubes as the electron source in such a triode structure compared to other techniques such as deposited or etched tips are that:

1. the diameter of the structures is controlled by the catalyst size [64,65],
2. the height is controlled by synthesis time [66],
3. the growth orientation can be controlled to be perpendicular to the substrate surface, and
4. the location of the nanotube/nanowire can be controlled by catalyst placement through using lithography.

Carbon nanotubes can be fabricated with a typical standard deviation in the diameter and height being 4.1% and 6.3%, respectively, leading to excellent emitter uniformity as determined by electrical measurements [64,67].

By integrating a gate onto a chip, the gate-to-emitter distance can be substantially reduced which decreases the voltage required for controlling electron emission to a few tens of volts. This subsequently reduces the power, complexity, and cost of the gate drive/modulation circuitry.

The self-aligned process developed for the carbon nanotube cathode, reported extensively by Gangloff et al. [68], begins with the fabrication of a sandwich structure containing a gate electrode on top of an insulator which in turn is on top of an emitter electrode. An array of 300 nm diameter holes (20 000 in total), with a pitch of 5  $\mu\text{m}$ , was patterned using e-beam lithography (as seen in figure 1.5.1.1a showing a single resist hole) on top of the sandwich. A reactive ion etching step using  $\text{SF}_6$  gas is used to isotropically etch the polysilicon gate to form an 800 nm aperture. The silicon dioxide insulator is then isotropically etched in buffered

hydrofluoric acid (Figure 1.5.1.1b). Both the gate and insulator are overetched to produce an undercut so as to prevent emitters from touching the gate and the silicon dioxide from being charged during field emission. A 15 nm thick conductive TiN layer (which prevents catalyst diffusion) is then deposited by sputtering, followed by 7 nm of Ni (Figure 1.5.1.1c). The resist hole defines the gate, insulator, and emitter position and thus these features are “self-aligning”. The unwanted TiN and Ni over the gate are then removed by lifting off the e-beam resist. Carbon nanotubes are then grown by PECVD using a mixture of  $C_2H_2$  and  $NH_3$  (54: 200 sccm, respectively) at 5 mbar, 675 °C, with a -600 V sample bias (Figure 1.5.1.1d). This process typically produces straight, vertically aligned carbon nanotubes (Figure 1.5.1.2a, deposition time 15 min).

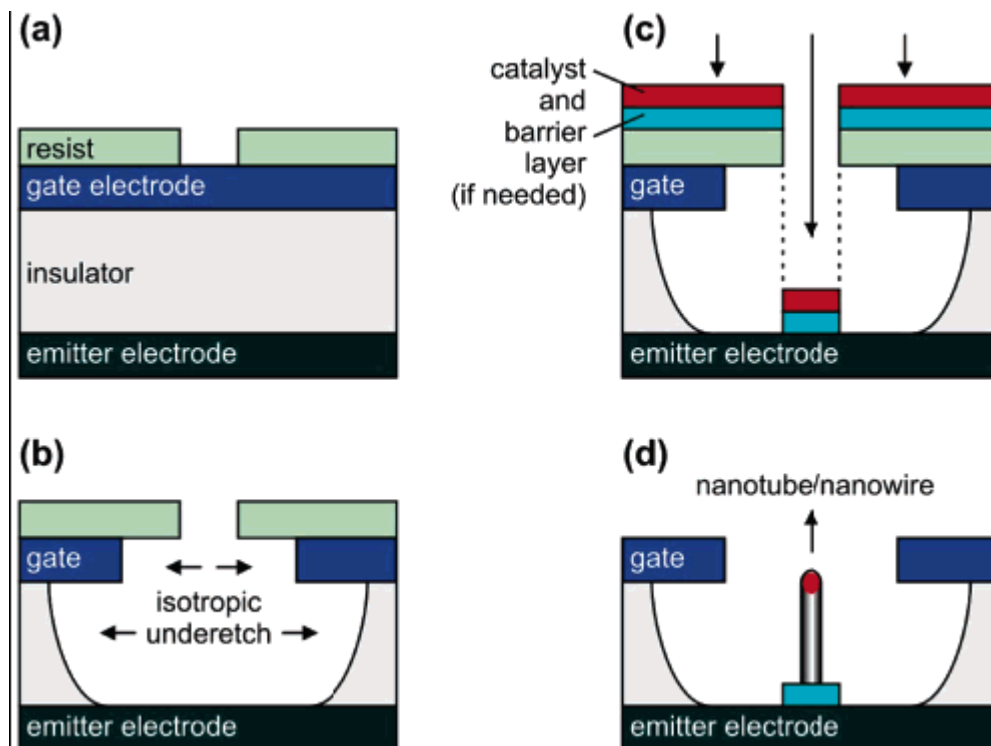


**Fig. 1.5.1.1.** The self-alignment process for fabricating an integrated gate with individual nanotube/nanowire cathodes. (a) A resist hole is first patterned onto a gate electrode/insulator/emitter electrode sandwich. (b) The gate and insulator material are then isotropically etched. (c) A thin film of catalyst, and diffusion barrier (if required), are deposited on the structure. (d) A lift-off is then performed to remove the unwanted catalyst on top of the gate followed by the nanotube/ nanowire growth inside the gate cavity.

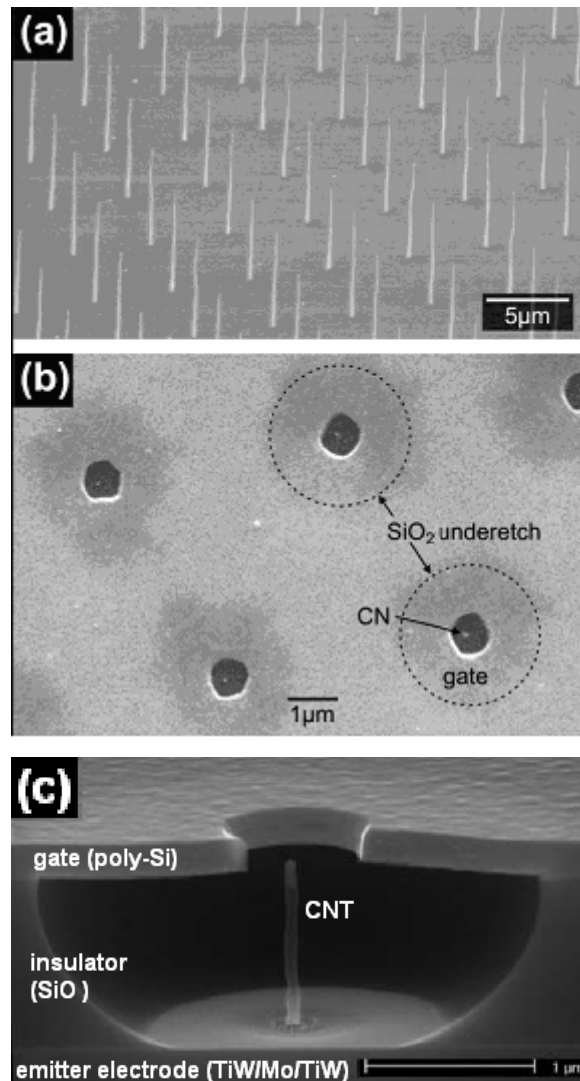


**Fig. 1.5.1.2.** (a) An array of carbon nanotubes, with a 5 μm pitch, deposited by PECVD of  $C_2H_2:NH_3$  at 675 °C for 15 min. (b) Top view of the integrated gate carbon nanotube cathode. The pitch of the gate apertures is 5 μm. The nanotube appears as a bright dot in each gate aperture. The dark contrast around the gate (within the dotted circle) arises from absence of the underlying  $SiO_2$  insulator which has isotropically underetched. (c) Cross section SEM view of the integrated gate carbon nanotube cathode, showing the gate electrode, insulator, emitter electrode, and vertically standing nanotube. The isotropic etching of the gate and the insulator prevent short circuits between the gate and emitter.

Figures 1.5.1.2b and 1.5.1.2c show the carbon nanotubes selectively grown inside the self-aligned gated structure. The deposition time was chosen to grow carbon nanotubes with their apex approximately equal in

---

height to the extraction gate (i.e., 1  $\mu\text{m}$ ) as this is the optimal configuration for gated cathodes [69].

The number of carbon nanotubes per aperture depends directly on the Ni catalyst dot size, with 7 nm thick Ni dots of 100 to 300 nm yielding a single nanotube 100%-88%, respectively [64]. The key advantages of this process are that no post-processing of the emitters is required and that the carbon nanotubes inside the gated cathode are essentially identical to those grown on a flat substrate.

Using a scanning anode field emission microscope (SAFEM), field emission measurements were performed on an integrated gate carbon nanotube cathode. The nanotube-based gated nanocathode array has a low turn-on voltage of 25 V and a peak current of 5  $\mu\text{A}$  at 46 V, with a gate current of 10 nA (i.e., 99% transparency). These low operating voltage cathodes are also potentially useful as electron sources for field emission displays or miniaturizing electron-based instrumentation.

Carbon nanotubes are an ideal electron source for such a novel parallel e-beam lithography system, but currently, more work is still needed to integrate a focusing grid into such a system.

## 1.5.2 ELECTRON GUN SOURCES

Electron microscopy demands a bright, stable, low-noise electron source with a low kinetic energy spread to maximise spatial resolution and contrast. Recent research has investigated whether the carbon nanotube can act as an improved electron source for this application and how it compares to other top-of-the-range electron sources available today.

### **1.5.2.1 STANDARD ELECTRON GUN SOURCES**

#### **1.5.2.1.1 LAB<sub>6</sub> EMITTERS**

LaB<sub>6</sub> emitters were the first to be commonly used in electron microscopy. They have a long lifetime (~2000 hours), are very stable and have a low workfunction of 2.4 eV. They operate thermionically, in the same way that tungsten does and can be tailored to certain applications during the fabrication process. However, they commonly have a large energy spread of 1 eV and are not very bright ( $10^7$  A/cm<sup>2</sup>SR). They are typically used as electron sources for e-beam lithography.

#### **1.5.2.1.2 THE TUNGSTEN THERMIONIC EMITTER**

Tungsten thermionic emitters in essence have virtually the same properties as LaB<sub>6</sub>. However, tungsten emitters only last for ~100 hours, whereas LaB<sub>6</sub> emitters can last for months. They also have a large source size ( $>10^4$  atoms) due to their shape, and are even less bright than LaB<sub>6</sub> emitters ( $10^6$  A/cm<sup>2</sup>SR).

However, they are favoured because of their simplicity of manufacture. The emitter consists of a wire filament bent into the shape of a hairpin which is attached to a thicker metal support. The filament operates at ~2700 K by resistive heating. The tungsten cathodes are widely used because they are both reliable and inexpensive. Lateral resolution is limited because the tungsten cathode current densities are only about 1.75 A/cm<sup>2</sup>.

#### **1.5.2.1.3 THE SCHOTTKY EMITTER**

The Schottky emitter is designed to operate within definite temperature boundaries over time. It consists of a single crystal tungsten wire etched to 150 nm with a source of zirconium oxide deposited lower down the tip. Under heat, the zirconium oxide diffuses to the tip. The temperature range is typically 1750-1800 K. The effect of the oxide is to lower the

workfunction from  $\sim 5$  eV to 2.3 eV. A low workfunction is desirable, as this will result in a lower kinetic energy spread at high temperatures. The resultant energy spread is low  $\sim 0.3$  eV and the source size typically 15 nm. It is brighter than both thermionic emitters with a typical brightness of  $5 \times 10^8$  A/cm<sup>2</sup>SR and has a stability of less than 1%. They also last a very long time (1-2 years is typical). Interestingly, Schottky emitters increase in noise with time (a typical timeframe being over the period of a year). The mechanics of this are not as yet clearly understood.

#### **1.5.2.1.4 COLD FIELD EMITTERS**

The main benefits of cold field emitters are a small virtual source size (typically of 3 nm in tungsten), a low energy spread of 0.2-0.3 eV, high brightness (typically  $10^9$  A/cm<sup>2</sup>SR) and a lifetime of over a year. These field emitters are commonly used in high resolution electron microscopes as they are bright and the kinetic energy spread is low. Tungsten is the most commonly used cold field emitter, but its major disadvantage is its poor stability, with the current varying by as much as 6%. There are two main reasons for tungsten's poor stability. Its affinity to water means it is easy to etch (a 5 M solution of NaOH is sufficient) but also means that water is adsorbed onto the tip which then lowers the workfunction and thus changes the amount of current that can be withdrawn from the tip for a specific externally applied voltage. Also, the metallic nature of the bonding in tungsten - metallic bonds are, in general, not as strong as covalent bonds - means that on application of the high electric field required to withdraw current, atoms on the tungsten tip are able to move around the tip (called electromigration). This changes the shape of the tip which results in an alteration of the field which in turn leads to current oscillation.

Typical tip characteristics are outlined in table 1.5.2.1.4 below.

**Table 1.5.2.1.4.** A summary of the various types of electron source. The cold field emitter refers to tungsten and the tungsten emitter values refer to its thermionic properties. Information courtesy of FEI Company, Oregon, USA.

	Schottky	Cold Field	LaB <sub>6</sub>	Tungsten
Source size (nm)	15	3	10 <sup>4</sup>	> 10 <sup>4</sup>
Energy spread (eV)	0.3-1.0	0.2-0.3	1.0	1.0
Brightness (A/cm <sup>2</sup> SR)	5 × 10 <sup>8</sup>	10 <sup>9</sup>	10 <sup>7</sup>	10 <sup>6</sup>
Short-term stability %	< 1	4-6	< 1	< 1
Service life	> 1 year	> 1 year	2000 hours	100 hours
Workfunction (eV)	~2.3	~4.5 eV	~2.5 eV	4.5 eV

### 1.5.2.2 TIP ALIGNMENT

It is important to have alignment of the tip, as any error in the beam alignment will be magnified through all the various lens corrections down the column.

### 1.5.2.3 THE CARBON NANOTUBE: PROPERTIES AND CURRENT FABRICATION TECHNIQUES

It is important to understand in more detail why carbon nanotubes are desirable for high-quality field emission sources. Detailed investigations were carried out by de Jonge et al. [70]. As well as determining the typical characteristics of field emitters such as brightness, spectral distribution, kinetic energy spread etc, it was also important to conclusively determine whether the emission was coming from the nanotube itself.

### 1.5.2.3.1 METHODS OF TIP FABRICATION

A forest of carbon nanotubes grown by Teo et al was placed in an electron microscope with a tungsten tip. Carbon glue was applied to the tungsten tip which was brought close to the carbon nanotubes (see Figure 1.5.2.3.1). On applying a potential difference between the tip and the carbon nanotube, one of the carbon nanotubes was attracted to the tungsten tip and attached itself to the tip after sticking to the carbon glue. When the tip was withdrawn, the nanotube split, resulting in a carbon nanotube attached to the side of the tip through which field emission measurements could be made.

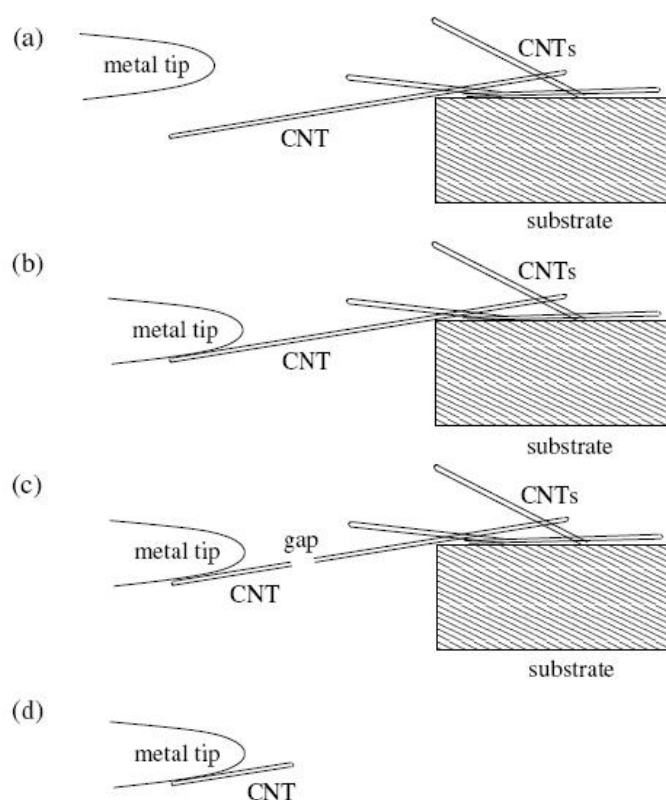


**Fig. 1.5.2.3.1.** A schematic of the carbon nanotube attachment process. a) shows a metal tip approaching a forest of randomly arranged nanotubes, b) shows a nanotube attached to the metal tip, c) shows the withdrawn tip splitting the carbon nanotube, d) is the resultant tip which is used for

measurement [71]. Reprinted with permission from AIP. © 2005 American Institute of Physics.

De Jonge attained the following field emission characteristics for CNTs outlined in table 1.5.2.3.1 below

**Table 1.5.2.3.1.** Field emission properties of CNTs collated from all of de Jonge's papers on this subject.

Reduced Brightness / (A/srm <sup>2</sup> V)	10 <sup>9</sup>
Energy Spread / eV	0.2 - 0.5
Short-term stability %	0.2
Running Temp / K	700 - 900
Vacuum Level / mBar	< 2×10 <sup>-8</sup>
Noise Percentage %	0.12
Source Size / nm	0.2

Though the emission characteristics of the CNT have been found to be extremely promising [72], the attachment process is extremely cumbersome; the length the CNT protrudes from the tip cannot be controlled, neither can the CNT's alignment, nor can it be certain what the contact between the nanotube and tungsten wire is.

PECVD is a much better method to use, as most of this process can be automated and the process is scalable (i.e. it is possible to grow many tips simultaneously). We describe three significant challenges that have been overcome. Riley et al. [73] have already shown that a forest of highly defective CNTs can be grown on a tungsten tip by thermal chemical vapor deposition (TCVD), but in order for electron beam equipment to work effectively, there must be only a single source of electrons, hence a single CNT. As CNTs grow from a catalyst particle, the first challenge is to place a single catalyst particle at the vertex of the tip by the simplest and most reproducible process possible. The second challenge is to ensure that the nanotube is aligned in-axis with the rest of the tungsten tip. The third challenge is to improve the quality of the nanotube formed

at the top of the tip. This can be achieved by employing a new technique first reported by Minoux et al. [74] where the CNTs are thermally annealed following deposition.

### 1.5.2.3.2 AN ALTERNATIVE FABRICATION PROCESS

In 2006, Mann et al. reported the growth of aligned CNTs directly onto tungsten tips [75]. Tungsten tips 125  $\mu\text{m}$  in diameter and approximately 10 mm long were etched to an apex radius of between 20 and 30 nm at Philips Research Laboratories (PRL), Eindhoven, The Netherlands. The tips were then placed in a sputter-coater, with their axis aligned perpendicularly to the plane of the sputter target. 15 nm ITO was deposited. ITO is required to act as a diffusion barrier, as metal catalyst deposited onto a bare tungsten wire will diffuse down crystal planes and into the tungsten itself when molten, thus preventing the formation of catalyst particles to nucleate CNT growth. Subsequently, the tips were then either placed into an evaporator, or kept in the sputter coater, and a 5 nm layer of Ni deposited. The tungsten wires were then cut to a length of  $\sim 8$  mm and placed in a fully automated Black Magic PECVD reaction chamber (Nanoinstruments Ltd) for CNT growth.

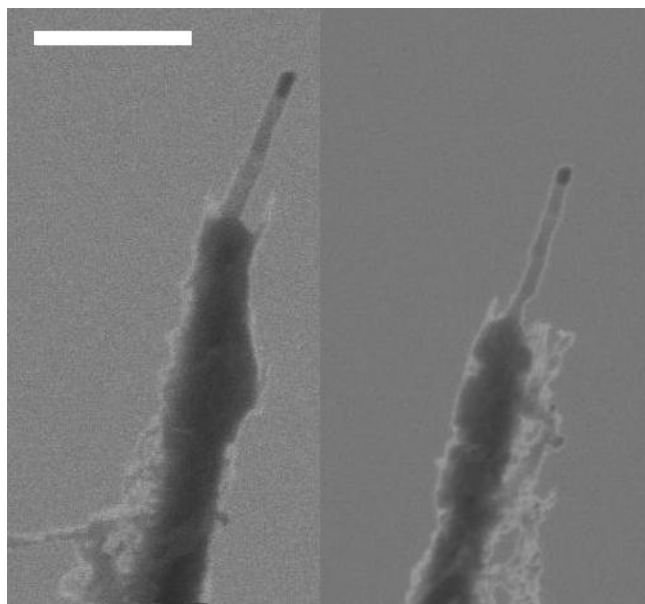


**Fig. 1.5.2.3.2.** left and right show single CNTs grown at the apex of sharp W tips. The scale bar is 200 nm. Ni catalyst particles can clearly be seen at the top of the CNTs. The Ni catalyst was deposited by sputter coating. Note that the CNTs are aligned with the axis of the tip [75].

The tips were ramped to 750 °C at 300 °C/min and NH<sub>3</sub> inlet at 120 sccm, raising the pressure to 2 mbar. Upon reaching 750 °C, C<sub>2</sub>H<sub>2</sub> was inlet at 30 sccm raising the total pressure to 3 mbar. A potential of 640 V was applied between the gas showerhead and the tip to initiate the plasma. The growth was performed for 15 minutes, producing CNTs of radius 20 nm and height 500 nm (as shown in figure 1.5.2.3.2).

CNTs may offer low-extraction voltage, high brightness solutions to electron microscopy demands. The challenge has been to develop a process to enable bringing CNT electron source devices to market. This fabrication method, scalable to mass production allows for the first time the direct deposition of aligned CNTs onto tungsten tips.

### **1.5.3 MICROWAVE AMPLIFIERS**

Microwave amplifiers are used extensively in satellites as transponders which at present are based on relatively inefficient thermionic electron sources that require heating and cannot be switched on instantaneously. After describing how current conventional microwave amplifiers operate, it will be shown how CNTs can be used to increase amplifier efficiency and response time whilst reducing their weight.

#### **1.5.3.1 CONVENTIONAL MICROWAVE AMPLIFIERS**

Currently, satellites employ the travelling wave tube, or TWT, to amplify a signal. Formerly, TWT was referred to as the travelling wave amplifier tube, but this term fell out of common usage for obvious reasons. The TWT was invented by Rudolf Kompfner during the Second World War, and was later refined by both Kompfner and John Pierce at Bell Labs [76][77]. The main elements of a travelling-wave tube (TWT) are an electron gun, which produces a beam of electrons that travels down a vacuum tube; a magnetic focusing structure that keeps the electrons in a linear path; an RF circuit that causes RF fields to interact with the

electron beam; and a collector with which to collect the electrons. This is shown in figure 1.5.3.1.

The electron beam, generated by a thermionic electron gun is focused in the vacuum tube by the magnetic focusing structure. The magnetic focusing structure produces either a uniform or spatially-varying magnetic field in the axial direction parallel to the propagation of the electron beam to constrain the beam as it passes through the vacuum tube. A directional coupler, which can be either a waveguide or an electromagnetic coil, is fed with the low-powered radio signal that is to be amplified, positioned near the emitter, and induces a current into the helix.

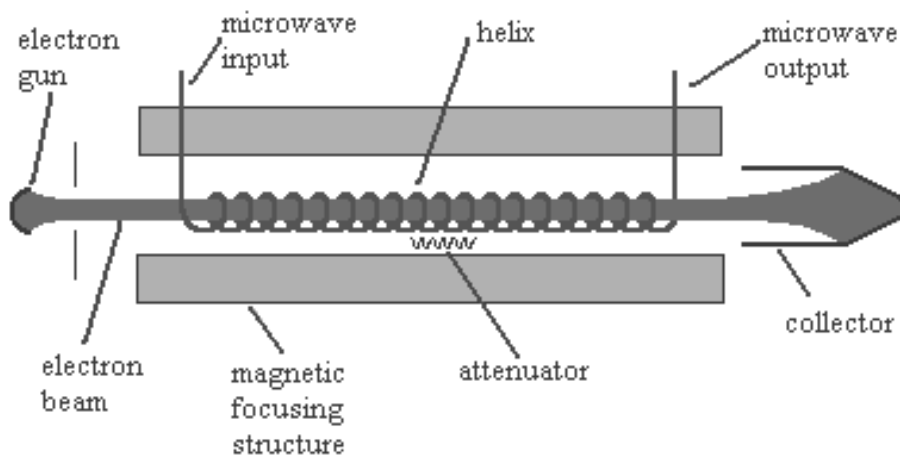


**Fig. 1.5.3.1.** Schematic diagram of a TWT. The device is an elongated vacuum tube with an electron gun (a heated cathode that emits electrons) at one end. A solenoid coil or system of permanent magnets (depending on the power of the device) is wrapped around the tube creating a magnetic field which focuses the electrons into a beam. The beam then passes down the middle of a wire helix that stretches the length of the tube, finally striking a collector at the other end.

The helix behaves as a delay line, in which the RF signal travels at the same speed along the tube as the electron beam. The current in the helix generates an electromagnetic field which interacts with the electron beam. The field either accelerates or retards the electrons in the beam dependent on the direction of the field generated. This causes bunching of the

electrons in an effect called velocity modulation. The electromagnetic field due to the beam current then induces more current back into the helix. Hence, the current builds up and is thus amplified as it passes down the helix.

A second directional coupler, positioned near the collector, receives an amplified version of the input signal from the far end of the helix. The attenuator prevents any reflected wave from travelling back to the cathode. This amplified output is then coupled to an antenna (e.g. a dish) for transmission thousands of miles back to earth. The bandwidth of a broadband TWT can be as high as one octave, although tuned (narrowband) versions exist, and operating frequencies range from 300 MHz to 50 GHz. The voltage gain of the tube can be of the order of 40 decibels. However, only 30% of the beam is converted to bunches with the efficiency even lower at higher frequencies. Conventional microwave amplifiers based on thermionic sources are approximately 30 cm long and weigh 1 kg.

### **1.5.3.2 CARBON NANOTUBES AS COLD MICROWAVE AMPLIFIERS**

An alternative method for microwave amplification reported recently [78] incorporates a microwave diode that instead uses a cold-cathode electron source consisting of a CNT array which operates at high frequency and at high current densities.

Sixteen CNT arrays individually occupying an area of  $0.5 \times 0.5 \text{ mm}^2$  and consisting of 2500 uniform carbon nanotubes with an average diameter of 49 nm, height of  $5.5 \text{ }\mu\text{m}$  and a spacing of  $10 \text{ }\mu\text{m}$  (with a standard deviation in diameter of 4% and a standard height deviation of 6%) [64] were integrated onto a silicon chip placed on a coaxial post in a resonant cavity. The CNTs are spaced at a distance corresponding to roughly twice their height in order to minimize the effects of electrostatic field shielding from adjacent emitters [79] whilst maximising the field emission current per unit area (Fig. 1.5.3.2, inset). The carbon nanotubes must also be well crystallized so that they have a high electrical conductivity. So a rapid thermal anneal after growth under high vacuum increases the graphitization of the nanotubes.

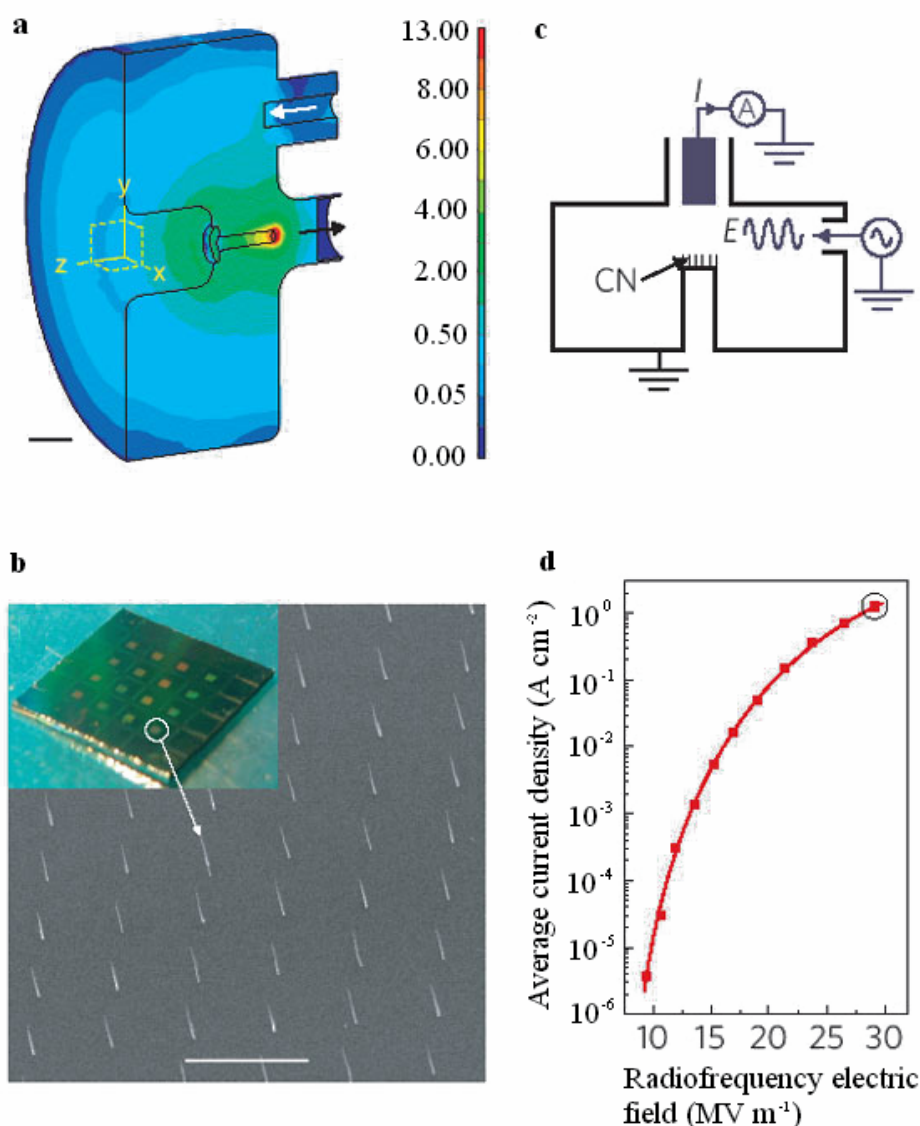


**Fig. 1.5.3.2.** Features of the carbon-nanotube microwave diode. a, Simulation of the coaxial resonant cavity (a cross-section is shown) that was used to generate a high electric field (red) at the carbon-nanotube-array cathode from the radiofrequency input; colour scale shows the applied macroscopic electric field in volts ( $\times 10^5$ ) per metre. White arrow, coaxial radiofrequency input; black arrow, emitted electron beam, collected by an antenna; scale bar 10 mm. b, Electron micrograph of the carbon-nanotube-array cold cathode at a tilt of  $45^\circ$ ; scale bar,  $15 \mu\text{m}$ . Inset, photograph of 16 cathodes. c, Representation of the equivalent electrical circuit, where E is the applied electric field and I is the emitted current; CNT, carbon nanotube array. d, Measured average current density plotted against applied radiofrequency electric field using 1.5-GHz sinusoidal input. The circled point corresponds to  $I = 3.2 \text{ mA}$ . The cavity-quality factor was 3,160 (see supplementary information) [78]. Reprinted by permission from Macmillan Publishers Ltd: Nature, © 2005.

This setup (shown in figure 1.5.3.2a, 1.5.3.2b and 1.5.3.2c) has the carbon-nanotube array acting as a cold cathode electron source. The source emits bunches of electrons directly by turning on and off in response to an input RF signal, in a process known as temporal modulation. The devices produced electron bunches with a peak current of  $12 \text{ A/cm}^2$  at a pulse frequency of 1.5 GHz, shown in figure 1.5.3.2d.

There is no need for heating (since carbon nanotubes are cold cathodes), no need for two-thirds of the length of the interaction tube (since the bunches are directly obtained from the carbon nanotubes), and the collector can be simplified as all electrons have the same velocity and fewer electrons are being dumped. With hot cathodes, there is a need for a multi-stage collector as the electrons have different speeds (i.e. are dispersed) from the inefficient bunching process.

In contrast, it is possible to directly generate RF beams (at GHz frequencies) of electrons from carbon nanotube arrays. Cambridge University Engineering Department, together with Thales, have successfully demonstrated the Class D (i.e. pulse mode/on-off) operation of a carbon nanotube array cathode at 1.5 GHz, with an average current density of  $1.3 \text{ A/cm}^2$  and peak current density of  $12 \text{ A/cm}^2$  [78]; these are compatible with traveling wave tube amplifier requirements ( $>1 \text{ A/cm}^2$ ). Recently, Cambridge have achieved 32GHz direct modulation of a carbon nanotube array cathode under Class A (i.e. sine wave) operation, with over 90% modulation depth. This unique ability to directly modulate or generate RF/GHz electron beams from carbon nanotube emitters is especially important for microwave devices as it essentially replaces the lengthy hot cathode and its associated modulation stage. Other advantages that the carbon nanotube cathode offer include no heating requirement and the ability to turn it on or off instantly (for efficient operation).

This carbon-nanotube cathode already delivers average and peak-current densities that are similar to those presently used in microwave transmission devices. The total expected size and weight reduction from the electron source, tube and collector is around 50%. This is highly significant because today, each communications satellite carries around 50 amplifiers. The size and weight savings would lead directly to more devices being carried on each satellite or lighter satellites with cheaper launch costs; it costs £10,000 to send 1 kg into space. Because of their small size, and their ability to generate and modulate the beam directly on demand without the need for high temperatures, CNT cathodes could be

employed in a new generation of lightweight, efficient and compact microwave devices for telecommunications in satellites or spacecraft.

## 1.6 SUMMARY

Micro and nano-structurally rich carbon materials are alternatives to conventional metal/silicon tips for field emission sources. In particular, carbon nanotubes exhibit extraordinary field emission properties because of their high electrical conductivity, ideal high aspect ratio whisker-like shape for geometrical field enhancement, and remarkable thermal stability. Combining microfabrication techniques with carbon nanotube growth by PECVD can produce well defined micro-electron sources and offer numerous integrated device possibilities for the future.

## 1.7 REFERENCES

- [1] Deuk-Seok Chung, S. H. Park, H. W. Lee, J. H. Choi, S. N. Cha, J. W. Kim, J. E. Jang, K. W. Min, S. H. Cho, M. J. Yoon, J. S. Lee, C. K. Lee, J. H. Yoo, Jong-Min Kim, J. E. Jung, Y. W. Jin, Y. J. Park, and J. B. You: *Appl. Phys. Lett.* Vol. 80 (2002), pp. 4045ff.
- [2] K.B.K. Teo, E. Minoux, L. Hudanski, F. Peauger, J.-P. Schnell, L. Gangloff, P. Legagneux, D. Dieumgard, G.A.J. Amaratunga and W.I. Milne: *Nature* Vol. 437 (2005), pp. 968ff.
- [3] N. de Jonge, M. Allieux, J.T. Oostveen, K.B.K. Teo and W.I. Milne: *Physical Review Letters* Vol. 94 (2005), pp. 186807ff.
- [4] W.I. Milne, K.B.K. Teo, E. Minoux, O. Groening, L. Gangloff, L. Hudanski, J.-P. Schnell, D. Dieumegard, F. Peauger, I.Y.Y. Bu, M.S. Bell, P. Legagneux, G. Hasko, and G.A.J. Amaratunga: *Journal of Vacuum Science and Technology B* Vol. 24 (2006), pp. 345ff.
- [5] Marcuccio, S., Genovese, A. & Andrenucci, M. 1997 FEED microthruster technology status and prospects. In *Proc. 48th Int. Astronautical Federation Cong.*, Turin, Italy. Paris: International Astronautical Federation.

- [6] C. A. Spindt: *J. Appl. Phys.* Vol. 39 (1968), pp. 3504ff; C. A. Spindt, I. Brodie, L. Humphrey and E. R. Westerberg: *J. Appl. Phys.* Vol. 47 (1976), pp. 5248ff.
- [7] From Pixtech's website, [www.pixtech.com](http://www.pixtech.com)
- [8] A. F. Bernhardt, R. J. Contolini, A. F. Jankowski, V. Liberman, J. D. Morse, R. G. Musket, R. Barton, J. Macaulay, and C. Spindt: *J. Vac. Sci. Tech. B* Vol. 18 (2000), pp. 1212ff.
- [9] Pictures from K. L. Jensen, "Theory and simulation of field emission from microstructures", <http://other.nrl.navy.mil/CREBWorkShop/Jensen.pdf>. Individual sources: Candescant/Sony DVD player – Chris Curtin; Motorola 15" FED – Alec Talin; NG/SRI TWT – David Whaley.
- [10] D. R. Whaley, B. M. Gannon, C. R. Smith, C. M. Armstrong, and C. A. Spindt: *IEEE Trans. Plasma Science* Vol. 28 (2000), pp. 727ff.
- [11] R. Fowler and L. Nordheim: *Proc. R. Soc. London, Ser. A* Vol. 119 (1928), pp. 173ff.
- [12] R.G. Forbes In: A.L. Suvorov, Yu.G. Abov and V.G. Firsov, Editors, *Proceedings of 4th Moscow International ITEP School of Physics*, Academprint, Moscow (2001), p. 62.
- [13] I. Brodie and C. Spindt: *Adv. Electron. Electron Phys.* Vol. 83 (1992), pp. 1ff.
- [14] F. S. Baker, A. R. Osborn, and J. Williams: *Nature* Vol. 239 (1972), pp. 96ff.
- [15] C. Wang, A. Garcia, D. C. Ingram, M. Lake, and M. E. Kordesch: *Electron Lett* Vol. 27 (1991), pp. 1459ff.
- [16] M. W. Geis, N. Efremow, J. Woodhouse, M. Mcalese, M. Marchywka, D. Socker, and J. Hochedez: *IEEE Elect. Dev. Lett.* Vol. 12 (1991), pp. 456ff.
- [17] B. C. Djubua, and N. N. Chubun: *IEEE Trans. Electron Dev.* Vol. 38 (1991), pp. 2314ff.
- [18] W. Zhu, G. P. Kochanski, S. Jin, and L. Seibles: *J. Appl. Phys.* Vol. 78 (1995), pp. 2707ff.
- [19] B. S. Satyanarayana, A. Hart, W. I. Milne and J. Robertson: *Appl. Phys. Lett.* Vol. 71 (1997), pp. 1430ff.

- 
- [20] G. A. J. Amaratunga and S. R. P. Silva: *Appl. Phys. Lett.* Vol. 68 (1996), pp. 2529ff.
- [21] A. N. Obraztsov, I. Yu. Pavlovsky and A. P. Volkov: *J. Vac. Sci. Tech. B*, Vol. 17 (1999), pp. 654ff.
- [22] A. N. Obraztsov, I. Pavlovsky, A. P. Volkov, E. D. Obraztsova, A. L. Chuvilin, and V. L. Kuznetsov: *J. Vac. Sci. Tech. B* Vol. 18 (2000), pp. 1059ff.
- [23] B. F. Coll, J. E. Jaskie, J. L. Markham, E. P. Menu, A. A. Talin, and P. von Allmen: *Mater. Res. Soc. Symp. Proc.* Vol. 498(1998), pp. 185ff.
- [24] B. S. Satyanarayana, J. Robertson and W. I. Milne: *J. Appl. Phys.* Vol. 87 (2000), pp. 3126ff.
- [25] G. A. J. Amaratunga, M. Baxendale, N. Rupesinghe, I. Alexandrou, M. Chhowalla, T. Butler, A. Munindradasa, C. J. Kiley, L. Zhang and T. Sakai: *New Diamond and Frontier Carbon Technology* Vol. 9 (1999), pp. 31ff.
- [26] Q. H. Wang, T. D. Corrigan, J. Y. Dai, R. P. H. Chang and A. R. Krauss: *Appl. Phys. Lett.* Vol. 70 (1997), pp. 3308ff.
- [27] I. Musa, D. A. I. Munindradasa, G. A. J. Amaratunga, and W. Eccleston: *Nature* Vol. 395 (1998), pp. 362ff.
- [28] M. W. Geis, J. C. Twichell and T. M. Lyszczarz: *Journal of Vacuum Science and Technology B*, Vol. 14 (1996), pp. 2060ff.
- [29] J. Robertson: *Diam. Relat. Mater.* Vol. 5 (1996), pp. 797ff.
- [30] J. Robertson and W. I. Milne: *Journal of Non Crystalline Solids* Vols. 227-230 (1998), pp. 558ff.
- [31] F. Lacher, C. Wild, D. Behr, and P. Koidl: *Diam. Relat. Mater.* Vol. 6 (1997), pp. 1111ff.
- [32] O. Groening, O. M. Kuettel, P. Groening, and L. Schlapbach: *J. Vac. Sci. Tech. B* Vol. 17 (1999), pp. 1970ff.
- [33] A. V. Karabutov, V. D. Frolov, S. M. Pimenov, and V. I. Konov: *Diam. Relat. Mater.* Vol. 8 (1999), pp. 763ff.,
- [34] O. Groening, O. M. Kuettel, E. Schaller, P. Groening, and L. Schlapbach: *Appl. Phys. Lett.* Vol. 69 (1996), pp. 476ff.
- [35] A. A. Talin, T. E. Felter, T. A. Friedmann, J. P. Sullivan, and M. P. Siegal: *J. Vac. Sci. Tech. A* Vol. 14 (1996), pp. 1719ff.

- [36] I. H. Shin and T. D. Lee: *J. Vac, Sci. Tech. B* Vol. 17 (1999), pp. 690ff.
- [37] K. B. K. Teo, S. E. Rodil, J. T. H. Tsai, A. C. Ferrari, J. Robertson, and W. I. Milne: *J. Appl. Phys.* Vol. 89 (2001), pp. 3706ff.
- [38] O. Groening, O. M. Kuettel, P. Groening, and L. Schlapbach: *Appl. Phys. Lett.* Vol. 71 (1997), pp. 2253ff.
- [39] J. T. H. Tsai, K. B. K. Teo, and W.I. Milne, *Materials Science and Engineering A*, accepted Sep 2001.
- [40] M. A. Guillorn, T. E. McKnight, A. Melechko, V. I. Merkulov, P. F. Britt, D. W. Austin, D. H. Lowndes, and M. L. Simpson: *J. Appl. Phys.* Vol. 91 (2002), pp. 3824ff.
- [41] M. A. Guillorn, A. V. Melechko, V. I. Merkulov, E. D. Ellis, C. L. Britton, M. L. Simpson, and D. H. Lowndes: *Appl. Phys. Lett.* Vol. 79 (2001), pp. 3506ff.
- [42] S. Ijima: *Nature* Vol. 354 (1991), pp. 56ff.
- [43] T. Utsumi: *IEEE Trans. Electron Dev.* Vol. 38(1991) , pp. 2276ff.
- [44] Y. Wei, C. Xie, K. A. Dean, and B. F. Coll: *Appl. Phys. Lett.* Vol. 79 (2001), pp. 4527ff.
- [45] Sources for pictures:
- Arc discharge carbon nanotubes – Q. H. Wang et al.: *Appl. Phys. Lett.* Vol. 70 (1997), pp. 3308ff;
- CVD spaghetti carbon nanotubes – grown using Fe(NO<sub>3</sub>) catalyst on Si substrate at 560°C under C<sub>2</sub>H<sub>2</sub> and NH<sub>3</sub>;
- PECVD carbon nanotubes – see chapter 3;
- Si whiskers by VLS – by P. Legagneux, also see E. I. Givargizov: *J. Vac. Sci. Tech. B* Vol. 11 (1993), pp. 449ff;
- Oxidation sharpened Si tips – M. Ding, H. Kim, and A. I. Akinwande: *IEEE Trans. Electron Dev.* Vol. 21 (2000), pp. 66ff;
- Spindt Mo tip – see ref. [2];
- ODE (orientation dependent etching) wet etched Si – H. Schroder, E. Obermeier, and A. Steckenborn: *J. Micromech. Microeng.* Vol. 9 (1999), pp. 139ff.
- CVD diamond from inverted Si molds - [http://pyramid.spd.louisville.edu/~eri/pages/news\\_nano.html](http://pyramid.spd.louisville.edu/~eri/pages/news_nano.html); see

- also W. P. Kang, A. Wisitor-at, J. L. Davidson, M. Howell, D. V. Kerns, Q. Li, J. F. Xu, and C. K. Kim: *J. Vac. Sci. Tech. B* Vol. 16 (1998), pp. 732ff.
- [46] S. T. Purcell, P. Vincent, C. Journet, and Vu Thien Binh: *Phys. Rev. Lett.* Vol. 88 (2002), pp. 105502ff.
- [47] Sources for pictures:
- (a), (b): [www.sidiamond.com](http://www.sidiamond.com), under ANI (Applied Nanotech Inc)
- (c), (d): [www.oxfordxtg.com](http://www.oxfordxtg.com)
- (e): W. B. Choi, D. S. Chung, J. H. Kang, H. Y. Kim, Y. W. Jin, I. T. Han, Y. H. Lee, J. E. Jung, N. S. Lee, G. S. Park, and J.M. Kim: *Appl. Phys. Lett.* Vol. 75 (1999), pp. 3129ff.
- (f): Deuk-Seok Chung, S. H. Park, H. W. Lee, J. H. Choi, S. N. Cha, J. W. Kim, J. E. Jang, K. W. Min, S. H. Cho, M. J. Yoon, J. S. Lee, C. K. Lee, J. H. Yoo, Jong-Min Kim, J. E. Jung, Y. W. Jin, Y. J. Park, and J. B. You: *Appl. Phys. Lett.* Vol. 80 (2002), pp. 4045ff.
- [48] Presentation at Materials Week 2001 by Matthieu Grac of Nanoledge, France.
- [49] W. B. Choi, Y. W. Jin, H. Y. Kim, S. J. Lee, M. J. Yun, J. H. Kang, Y. S. Choi, N. S. Park, N. S. Lee, and J. M. Kim: *Appl. Phys. Lett.* Vol. 78 (2001), pp. 1547ff.
- [50] T. W. Ebbesen, P. W. Ayajan: *Nature* Vol. 358 (1992), pp. 220.
- [51] Guo et al.: *J. Phys. Chem.* Vol. 99, pp. 10694ff.
- [52] P. G. Collins and P. Avouris: *Scientific American* December 2000, 67 (2000)
- [53] R. T. K. Baker: *Carbon* Vol. 27 (1989), pp. 315ff.
- [54] V. I. Merkulov, D. H. Lowndes, Y. Y. Wei, G. Eres, and E. Voelkl: *Appl. Phys. Lett.* Vol. 76 (2000), pp. 3555ff.
- [55] C. Bower, O. Zhou, W. Zhu, D. J. Werder, and S. Jin: *Appl. Phys. Lett.* Vol. 77 (2000), pp. 2767ff.
- [56] J. I. Sohn, C. -J. Choi, T. -Y. Seong, and S. Lee: *Mat. Res. Symp. Proc.* Vol. 706 (2002), pp. Z3.8.1ff.
- [57] S. Fan, M. Chapline, N. Franklin, T. Tomblor, A. Cassell, H. Dai: *Science* Vol. 283 (1999), pp. 512ff.

- [58] J.-M. Bonard, T. Stöckli, O. Noury, A. Chatelain: *Appl. Phys. Lett.* Vol. 78 (2001), pp. 2775ff.
- [59] Rosen, R.; Simendinger, W.; Debbault, C.; Shimoda, H.; Fleming, L.; Stoner, B.; Zhou, O.: *Appl. Phys. Lett.* Vol. 76 (2000), pp. 1668ff.
- [60] Sugie, H., Tanemure, M., Filip, V., Iwata, K., Takahashi, K. & Okuyama, F.: *Appl. Phys. Lett.* Vol. 78 (2001), pp. 2578ff.
- [61] Choi, W. B. (and 10 others): *Appl. Phys. Lett.* Vol. 75 (1999), pp. 3129ff.
- [62] Niels de Jonge and Jean-Marc Bonard: *Phil. Trans. R. Soc. Lond. A* Vol. 362 (2004), pp. 2239ff.
- [63] W. I. Milne, K. B. K. Teo, G. A. J. Amaratunga, P. Legagneux, L. Gangloff, J.-P. Schnell, V. Semet, V. Thien Binh and O. Groening: *J. Mater. Chem.* Vol. 14 (2004), pp. 1ff.
- [64] Teo, K. B. K.; Lee, S.-B.; Chhowalla, M.; Semet, V.; Binh, V. T.; Groening, O.; Castignolles, M.; Loiseau, A.; Pirio, G.; Legagneux, P.; Pribat, D.; Hasko, D. G.; Ahmed, H.; Amaratunga, G. A. J.; Milne, W. I.: *Nanotechnology* Vol. 14 (2003), pp. 204ff.
- [65] Cui, Y.; Lauhon, L. J.; Gudixsen, M. S.; Wang, J.; Lieber, C. M.: *Appl. Phys. Lett.* Vol. 78 (2001), pp. 2214ff.
- [66] Chhowalla, M.; Teo, K. B. K.; Ducati, C.; Rupesinghe, N. L.; Amaratunga, G. A. J.; Ferrari, A. C.; Roy, D.; Robertson, J.; Milne, W. I.: *J. Appl. Phys.* Vol. 90 (2001), pp. 5308ff.
- [67] Semet, V.; Vu, T. B.; Vincent, P.; Guillot, D.; Teo, K. B. K.; Chhowalla, M.; Amaratunga, G. A. J.; Milne, W. I.; Legagneux, P.; Pribat, D.: *Appl. Phys. Lett.* Vol. 81 (2002), pp. 343ff.
- [68] L. Gangloff, E. Minoux, K. B. K. Teo, P. Vincent, V. T. Semet, V. T. Binh, M. H. Yang, I. Y. Y. Bu, R. G. Lacerda, G. Pirio, J. P. Schnell, D. Pribat, D. G. Hasko, G. A. J. Amaratunga, W. I. Milne, and P. Legagneux: *Nanoletters* Vol. 4 (2004), pp. 1575ff.
- [69] Spindt, C. A.; Brodie, I.; Humphrey, L.; Westerberg, E.: *J. Appl. Phys.* Vol. 47 (1996), pp. 5248ff.
- [70] N. de Jonge, M. Allieux, J.T. Oostveen, K.B.K. Teo and W.I. Milne: *Physical Review Letters* Vol. 94 (2005), pp. 186807ff.

- 
- [71] N de Jonge, M Doytcheva, M Allieux, M Kaiser, S. A. M. Mentink, K. B. K. Teo, R. G. Lacerda, W. I. Milne: *Advanced Materials* Vol. 17 (2005), pp. 451ff.
- [72] A. Javey, Q. Wang, A. Ural, Y. Li, H. Dai: *Nano Letters* Vol. 2 (2002), pp. 929ff.
- [73] David J. Riley, Mark Mann, Donald A. MacLaren, Paul C. Dastoor, William Allison, Kenneth B. K. Teo, Gehan A. J. Amaratunga and William Milne: *Nano Letters* Vol. 3 (2003), pp. 1455ff.
- [74] E. Minoux, O. Groening, K. B. K. Teo, S. H. Dalal, L. Gangloff, J-P Schnell, L. Hudanski, Ian Y. Y. Bu, . Vincent, P. Legagneux, G. A. J. Amaratunga, and W. I. Milne: *Nanoletters* Vol. 5 (2005), pp. 2135ff.
- [75] M. Mann, K. B. K. Teo, W. I. Milne, T. Tessner: *Nano: Brief Reports and Reviews: Vol. 1* (2006), pp. 35ff.
- [76] Pierce, John R. (1950). *Traveling-Wave Tubes*. D. van Nostrand Co..
- [77] Kompfner, Rudolf (1964). *The Invention of the Traveling-Wave Tube*. San Francisco Press.
- [78] Kenneth B. K. Teo, Eric Minoux, Ludovic Hudanski, Franck Peauger, Jean-Philippe Schnell, Laurent Gangloff, Pierre Legagneux, Dominique Dieumegard, Gehan A. J. Amaratunga, William I. Milne: *Nature* Vol. 437 (2005), pp. 968ff.
- [79] Nilsson, L. et al.: *Appl. Phys. Lett.* Vol. 76 (2000), pp. 2071ff.